Raman-shifted alexandrite laser for soft tissue ablation in the 6- to 7-µm wavelength range

John Kozub,[1] Borislav Ivanov,[1] Aroshan Jayasinghe,[1] Ratna Prasad,[2] Jin Shen,[2] Marc Klosner,[3] Donald Heller,[3] Marcus Mendenhall,[1] David W. Piston,[1,4,5] Karen Joos,[2] and M. Shane Hutson[1,6,*]

[1]*Department of Physics & Astronomy, Vanderbilt University, Nashville, TN 37235, USA*
[2]*Vanderbilt Eye Institute, Vanderbilt University, Nashville, TN 37232, USA*
[3]*Light Age, Inc., 500 Apgar Drive, Somerset, NJ 08873, USA*
[4]*Department of Molecular Physiology & Biophysics, Vanderbilt University, Nashville, TN 37232, USA*
[5]*Department of Biomedical Engineering, Vanderbilt University, Nashville, TN 37235, USA*
[6]*Vanderbilt Institute for Integrative Biosystem Research & Education, Nashville, TN 37235, USA*
*shane.hutson@vanderbilt.edu

Abstract: Prior work with free-electron lasers (FELs) showed that wavelengths in the 6- to 7-µm range could ablate soft tissues efficiently with little collateral damage; however, FELs proved too costly and too complex for widespread surgical use. Several alternative 6- to 7-µm laser systems have demonstrated the ability to cut soft tissues cleanly, but at rates that were much too low for surgical applications. Here, we present initial results with a Raman-shifted, pulsed alexandrite laser that is tunable from 6 to 7 µm and cuts soft tissues cleanly—approximately 15 µm of thermal damage surrounding ablation craters in cornea—and does so with volumetric ablation rates of $2–5 \times 10^{-3}$ mm^3/s. These rates are comparable to those attained in prior successful surgical trials using the FEL for optic nerve sheath fenestration.

OCIS codes: (140.3070) Infrared and far-infrared lasers; (140.3550) Lasers, Raman; (140.2600) Free-electron lasers (FELs); (170.1020) Ablation of tissue

References and links

1. G. Edwards, R. Logan, M. Copeland, L. Reinisch, J. Davidson, B. Johnson, R. Maciunas, M. Mendenhall, R. Ossoff, J. Tribble, J. Werkhaven, and D. O'Day, "Tissue ablation by a free-electron laser tuned to the amide II band," Nature **371**(6496), 416–419 (1994).
2. J. I. Youn, P. Sweet, G. M. Peavy, and V. Venugopalan, "Mid-IR laser ablation of articular and fibro-cartilage: a wavelength dependence study of thermal injury and crater morphology," Lasers Surg. Med. **38**(3), 218–228 (2006).
3. K. M. Joos, L. A. Mawn, J. H. Shen, E. D. Jansen, and V. A. Casagrande, "Acute optic nerve sheath fenestration in humans using the free electron laser (FEL): a case report," Proc. SPIE **4611**, 81–85 (2002).
4. R. A. Hill, Q. Ren, D. C. Nguyen, L. H. Liaw, and M. W. Berns, "Free-electron laser (FEL) ablation of ocular tissues," Lasers Med. Sci. **13**(3), 219–226 (1998).
5. G. S. Edwards, R. H. Austin, F. E. Carroll, M. L. Copeland, M. E. Couprie, W. E. Gabella, R. F. Haglund, B. A. Hooper, M. S. Hutson, E. D. Jansen, K. M. Joos, D. P. Kiehart, I. Lindau, J. Miao, H. S. Pratisto, J. H. Shen, Y. Tokutake, A. F. G. van der Meer, and A. Xie, "Free-electron-laser-based biophysical and biomedical instrumentation," Rev. Sci. Instrum. **74**(7), 3207–3245 (2003).
6. M. L. Copeland, R. J. Maciunas, and G. S. Edwards, "Use of the free-electron laser for metastatic brain tumors," in *Advanced Techniques in Central Nervous System Metastases*, R. J. Maciunas, ed., Neurosurgical Topic Series (The American Association of Neurological Surgeons, Park Ridge, IL, 1998).
7. K. M. Joos, L. A. Mawn, J. H. Shen, E. D. Jansen, R. D. Robinson, M. A. Mackanos, J. A. Mavity-Hudson, and V. A. Casagrande, "Human optic nerve sheath fenestration with the free electron laser (FEL)," Invest. Ophthalmol. Vis. Sci. 45, E-Abstract 45 (2004).
8. G. Edwards, M. S. Hutson, S. Hauger, J. Kozub, J. Shen, C. Shieh, K. Topadze, and K. A. Joos, "Comparison of OPA and Mark-III FEL for tissue ablation at 6.45 microns," Proc. SPIE **4633**, 194–200 (2002).
9. M. A. Mackanos, B. Ivanov, A. N. Soldatov, I. Kostadinov, M. H. Mendenhall, D. W. Piston, R. F. Haglund, and E. D. Jansen, "Ablation of soft tissue at 6.45 µm using a strontium vapor laser," Proc. SPIE **5319**, 201–208 (2004).

10. M. A. Mackanos, D. Simanovskii, K. M. Joos, H. A. Schwettman, and E. D. Jansen, "Mid infrared optical parametric oscillator (OPO) as a viable alternative to tissue ablation with the free electron laser (FEL)," Lasers Surg. Med. **39**(3), 230–236 (2007).
11. G. S. Edwards, R. D. Pearlstein, M. L. Copeland, M. S. Hutson, K. Latone, A. Spiro, and G. Pasmanik, "6450 nm wavelength tissue ablation using a nanosecond laser based on difference frequency mixing and stimulated Raman scattering," Opt. Lett. **32**(11), 1426–1428 (2007).
12. S. Wada, H. Tashiro, Y. Urata, L. T. Thi, A. Kasai, and K. Toyoda, "Two-stage Raman convertor covering the whole infrared spectrum with tunable solid-state lasers," Appl. Phys. B **57**(6), 435–439 (1993).
13. K. M. Joos, L. A. Mawn, J. H. Shen, and V. A. Casagrande, "Chronic and acute analysis of optic nerve sheath fenestration with the free electron laser in monkeys," Lasers Surg. Med. **32**(1), 32–41 (2003).
14. K. M. Joos, R. J. Shah, R. D. Robinson, and J. H. Shen, "Optic nerve sheath fenestration with endoscopic accessory instruments versus the free electron laser (FEL)," Lasers Surg. Med. **38**(9), 846–851 (2006).
15. R. J. Shah, J. H. Shen, and K. M. Joos, "Endoscopic free electron laser technique development for minimally invasive optic nerve sheath fenestration," Lasers Surg. Med. **39**(7), 589–596 (2007).
16. J. H. Shen, J. A. Harrington, G. S. Edwards, and K. M. Joos, "Hollow-glass waveguide delivery of an infrared free-electron laser for microsurgical applications," Appl. Opt. **40**(4), 583–587 (2001).

1. Introduction

Although lasers are in routine use across multiple medical specialties, no laser has yet made a widespread impact in precision neurosurgery. One candidate, mid-infrared (mid-IR) free-electron lasers (FELs), showed much promise and certainly can ablate soft biological tissues with high efficiency and remarkably little collateral damage [1–4]. In fact, work with the Vanderbilt FEL progressed to the successful completion of two FDA trials, encompassing eight human surgeries [5–7]. These surgeries—partial resection of intracranial tumors and fenestration of the optic nerve in blind eyes scheduled for enucleation—were considered major successes; however, the cost, size and complexity of an FELs' accelerator technology all but eliminates FELs' potential for widespread surgical use.

Recognizing this limitation, researchers have developed and evaluated multiple alternative laser systems. Since the optimal wavelength for FEL ablation was 6.0, 6.1 or 6.45 µm (variable between tissue types and research groups) [1–4], the alternative laser systems have all targeted the 6- to 7-µm wavelength range. Initial trials with picosecond optical parametric oscillators (OPOs) [8] and with Sr vapor lasers [9] both proved unsuccessful because neither had sufficient energy to generate single-pulse, thermally confined ablation. More recent trials have demonstrated the ability to ablate soft tissues with little collateral damage. These include an Er:YAG-pumped OPO system [10] and a Nd:YLF-based system that generates mid-IR light using a combination of stimulated Raman scattering and difference frequency mixing [11]. As noted by Edwards et al, the limitation of these latter two systems is that "the average optical power will need to increase by about *two orders of magnitude* to achieve sufficient ablation rates for human surgery [11]." Here, we present a robust Raman-shifted alexandrite (RSA) laser system with tunable operation across the entire 6- to 7-µm wavelength range, and demonstrate its capability to ablate soft tissues with less than 15 µm of collateral damage while removing tissue at rates comparable to prior human surgeries [5–7].

2. Experiments

This RSA laser system consists of a tunable, Q-switched alexandrite laser (101-PAL, Light Age Inc., Somerset, NJ) that pumps a two-stage Raman convertor (Fig. 1A) [12]. The fundamental output of the alexandrite laser is tuned to operate at wavelengths from 771 to 785 nm (ω_0 = 12740-12970 cm^{-1}) and directly pumps a deuterium-filled Raman convertor. In this first convertor, fundamental output of the alexandrite laser interacts with the D-D stretching mode of the deuterium gas (Ω_{D2} = 2991 cm^{-1}) by the nonlinear process of stimulated Raman scattering. This double-pass Raman convertor is designed to optimize production of 1st order Stokes'-shifted output near 1.01 µm (the exact wavelength determined by the tuning of the alexandrite fundamental, $\omega_1 = \omega_0 - \Omega_{D2}$). This nominal 1.01-µm output in turn pumps a hydrogen-filled Raman convertor. In this second convertor, multiple passes are used so that stimulated Raman scattering from the hydrogen gas (Ω_{H2} = 4155 cm^{-1}) terminally produces 2nd order Stokes'-shifted output with a wavelength in the 6- to 7-µm range ($\omega_2 = \omega_1 - 2\Omega_{H2}$).

Figure 1A shows the wavelengths used at each stage to produce output at 6.10 and 6.45 μm, wavelengths corresponding to two strong absorption bands of soft tissues. Line spectra for each of these outputs are shown in Fig. 1B. In typical operation, the alexandrite laser produces 250-mJ fundamental pulses at 10 Hz that are first converted to ~50-mJ pulses of nominally 1.01-μm light and subsequently converted to 1- to 3-mJ pulses in the 6- to 7-μm wavelength range. The alexandrite laser is capable of generating higher pulse energies (>400 mJ) and higher conversion efficiency can be attained with the deuterium convertor, but we limit the input to the multi-pass hydrogen convertor to avoid damaging its mirrors. Under optimal conditions, the RSA system used here has attained pulse energies up to 4 mJ at a wavelength of 6.1 μm. A second prototype RSA system has attained up to 9 mJ at 6.1 μm. During the nonlinear Raman conversion process, the 50-ns pulsewidth of the alexandrite laser is shortened to 10-20 ns while the spatial mode structure remains smooth and nearly Gaussian.
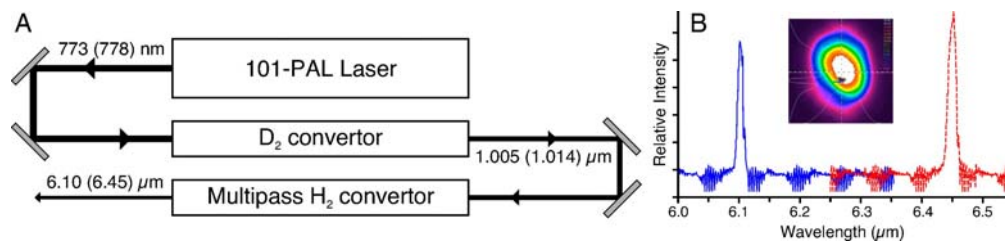

Fig. 1. Laser system schematic and characteristics. (**A**) A tunable alexandrite laser (PAL-101) pumps a two-stage Raman converter. As examples, alexandrite laser output at 773 or 778 nm undergoes a 1st order Stokes' shift in the deuterium (D_2) convertor to yield 1.005- or 1.014-μm light. This output then undergoes a terminal 2nd order Stokes' shift in the multi-pass hydrogen (H_2) convertor to yield light at 6.10 or 6.45 μm. Tunable output anywhere from 6 to 7 μm is achieved by tuning the alexandrite laser from 771 to 785 nm. (**B**) Spectra of the laser system output when tuned to 6.1 μm (*solid, blue*) or 6.45 μm (*dashed, red*). The inset shows a nearly Gaussian beam profile obtained at 6.3 μm; similar profiles are obtained from 6 to 7 μm.

As shown in Fig. 1, the RSA consists of three modules: an alexandrite pump laser (101-PAL) that employs an oscillator-amplifier configuration; a deuterium convertor; and a hydrogen convertor (all from Light Age). To enhance conversion efficiency, the deuterium convertor is operated in a double-pass configuration and the hydrogen convertor is operated with a high number of passes. This multi-pass configuration is needed to achieve efficient conversion even with a relatively low Raman gain coefficient in the 6- to 7-μm wavelength region. The resonator and beam delivery system use kinematically mounted optical components, providing excellent long-term stability despite a very long optical path length. The laser wavelength is easily tuned via an externally mounted micrometer, and the alignment is fully maintained when scanning the wavelength over the operating range of 6-7 μm.

To ensure consistency in tissue ablation studies, we warm-up the laser for approximately one hour prior to our experiments, allowing all components to become thermally stabilized. After warm-up, we characterize the spatial profile of the beam with burn paper and monitor the time-dependent output with a fast photodiode. We also measure the output energy from the deuterium convertor and the multi-pass convertor using a thermopile-based power meter (30A-P, Ophir-Spiricon Inc., Logan, UT) and a pyroelectric energy meter (J25, Coherent-Molectron Inc., Santa Clara, CA), respectively. Finally, we verify proper alignment through the multi-pass converter by means of an IR camera (Pyrocam III, Ophir-Spiricon)

For optimal performance of the current multi-pass convertor, the convertor is periodically baked, purged and refilled with hydrogen to eliminate residual water vapor that builds-up in concentration over time. Water vapor has very strong absorption in the 6- to 7-μm wavelength range and even very minute amounts have an observable effect on conversion efficiency—most prominently at mid-IR wavelengths corresponding to water vapor lines. We are developing new multi-pass convertor designs to minimize water vapor contamination. To maintain optimal performance, we also periodically refill the gas in the deuterium convertor.

3. Results and Discussion

In typical daily operation at 1- to 3-mJ per pulse and with moderate focusing to spot diameters of 180-300 μm, the RSA laser system is capable of ablating soft tissues and soft tissue models at substantial rates. Figure 2A shows an OCT (optical coherence tomography) image of nine partial thickness craters ablated in a gelatin model. Each crater was ablated using 160 pulses delivered at 10 Hz with a wavelength of 6.1 μm, pulse energy of 1.70 mJ and beam diameter of 300 μm (mean fluence of 0.60 J/cm^2). The average crater depth is 440 μm,
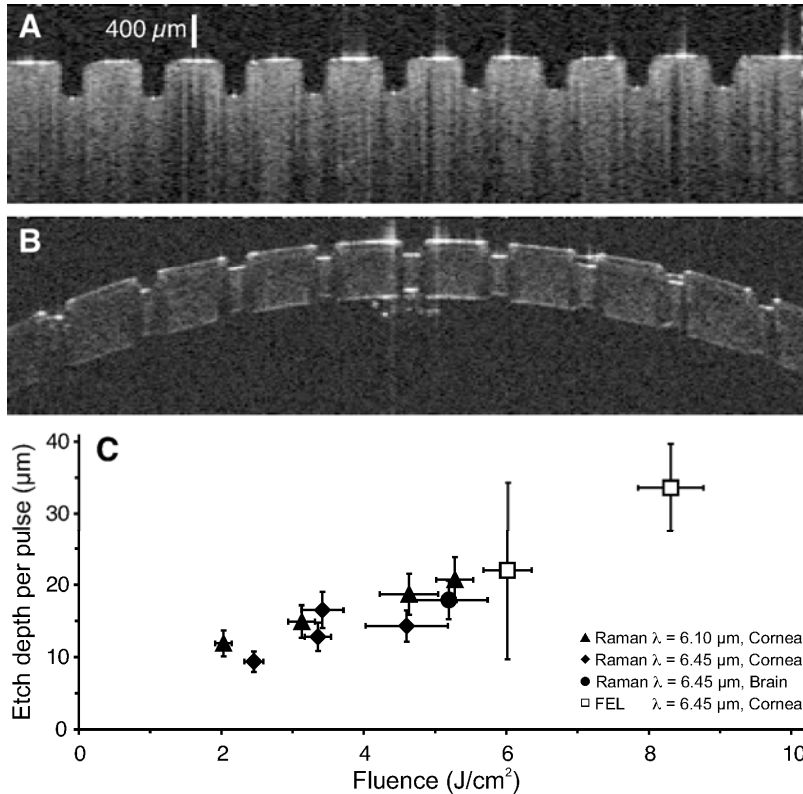

Fig. 2. Etch depths for partial and full thickness craters in soft tissues and soft tissue models. (**A**) OCT image of gelatin (10% wt/wt) ablated at λ = 6.1 μm with 160 pulses per crater (1.70 mJ/pulse at 10 Hz with a 300-μm beam diameter). The average depth of the craters is 440 μm with a standard deviation of ~5%. (**B**) OCT image of goat cornea ablated at λ = 6.1 μm with 40 pulses per crater (1.85 mJ/pulse at 10 Hz with a 300-μm beam diameter). The average depth of the craters is 163 μm. Note that the distortions along the inside surface of the cornea are OCT artifacts. The vertical scale bar applies to both images. (**C**) Mean etch depth per pulse achieved during full thickness ablations of porcine corneas (450- or 850-μm thick) or supported slices of freshly excised canine brain (1-mm thick) using λ = 6.1 or 6.45 μm with 0.5-1.3 mJ/pulse at 10 Hz. Two data points from FEL ablation of cornea are included for comparison.

corresponding to an average etch depth of 2.8 μm per pulse and an ablation rate of 28 μm/s (or 1.9 × 10^{-3} mm^3/s volumetrically). Since gelatin models may not fully capture all aspects of the laser-tissue interaction, Fig. 2B shows a similar OCT image after ablation of a goat cornea (still attached to an excised globe). In this case, just 40 pulses at slightly higher pulse energy—1.85 mJ or a fluence of 0.65 J/cm^2—ablated craters with an average depth of 163 μm, corresponding to an average etch depth of 4.1 μm per pulse and an ablation rate of 41 μm/s. These craters are not as wide as those in gelatin, so the volumetric ablation rate is only 1.8 × 10^{-3} mm^3/s. Figure 2C then shows ablation rates for the RSA laser based on the time required to perforate tissue slices of varying thickness. With slightly tighter focusing (beam

diameter of 180 μm), we reached fluences of 2-6 J/cm^2 that ablated cornea at 10-20 μm per pulse (an estimated 2.5-5.1 × 10^{-3} mm^3/s volumetrically) and brain at 18 μm per pulse (an estimated 4.6 × 10^{-3} mm^3/s volumetrically). These results are summarized in Table 1.

These ablation rates should be compared to those achievable with other 6- to 7-μm laser sources and with the rates used in previous FEL-based surgeries. The Nd:YLF based system developed by Passat Inc. and Duke University was able to ablate fixed brain tissue at just over 1 μm per pulse [11]; however, the laser's low 0.5-Hz repetition rate yielded an average ablation rate of just 0.64 μm/s or 5.0 x 10^{-6} mm^3/s, volumetrically (based on the stated spot diameter of 100 μm). Edwards et al estimated that surgical relevance would be reached at ablation rates that were two orders of magnitude higher [11]. A 10× improvement in volumetric ablation rate was demonstrated by the Er:YAG-pumped OPO developed at Stanford (Table 1) [10], but as shown here, the RSA laser is the first FEL alternative in the 6- to 7-μm wavelength range to achieve ablation rates with potential surgical relevance—due to a 400-1000× improvement in the volumetric ablation rate. The volumetric ablation rate is the one that needs to be compared to surgical procedures that require anything besides the drilling of a single small hole. For example, in optic nerve sheath fenestration, a window is cut in the optic nerve sheath by scanning the beam to make an incision along the circumference of a circle (diameter 2-3 mm) that completely incises the sheath (thickness 150-250 μm, depending on species). The unattached circle of nerve sheath is then removed manually. When this procedure was performed using the FEL, the beam diameter was approximately 200 μm and the lasing was completed in 2-3 minutes, so that the average volumetric ablation rate was 1-4 × 10^{-3} mm^3/s [3,7,13]. The present RSA laser can achieve this volumetric ablation rate with free-beam delivery, but may fall just short when fiber-coupling losses are included (as necessary for endoscopic delivery of the beam behind the eye [14,15]). The other procedure for which FDA trials were conducted with the FEL was partial excision of intracranial tumors. This procedure used higher fluences and ablated tumors at impressively high rates up to 2.0 × 10^{-2} mm^3/s [5]—placing it just out of reach (factor of ~4) of what we have thus far attained using free-beam delivery of the RSA laser.

Table 1. Ablation characteristics of pulsed laser systems operating in the 6- to 7-μm wavelength range[a]

Laser	λ μm	E mJ	w μm	f Hz	Tissue	δ μm	$d\delta/dt$ μm/s	dV/dt mm^3/s
RS-DFM-Nd:YLF [11]	6.45	<2	100	0.5	brain	1.3	0.64	5.0 × 10^{-6}
Er:YAG/OPO [10]	6.10 6.45	<0.25	60	5	cornea	3.8– 4.4	19-22	5.4 × 10^{-5} – 6.2 × 10^{-5}
RSA	6.10	1.7	300	10	gelatin	2.8	28	1.9 × 10^{-3}
	6.10	1.85	300	10	cornea	4.1	41	2.9 × 10^{-3}
	6.10 6.45	0.5-1.3	180	10	cornea	10–20	100– 200	2.5 × 10^{-3}– 5.1 × 10^{-3}
	6.45	1.3	180	10	brain	18	180	4.6 × 10^{-3}

[a]λ = wavelength, E = pulse energy, w = spot diameter, f = pulse repetition rate, δ = mean etch depth per pulse, $d\delta/dt$ = linear ablation rate and dV/dt = volumetric ablation rate

Improving the ablation rate would be moot if the RSA laser left behind excessive collateral damage, but initial histology of cornea, heart, skin and kidney ablated with the RSA laser shows that ablation is accompanied by only a very thin layer of thermally damaged tissue (Fig. 3). This damaged layer is clearest in cornea, where it is on average 15-μm thick. In the other tissues, the damaged layer is thinner and in some cases not even measureable (e.g. heart or kidney in Fig. 3B,D). These ablations were conducted either with free beam delivery of the laser (Fig. 3A) or with delivery via a hollow-glass waveguide and handheld probe (Fig. 3B-D) [16]. In the case of fiber optic delivery, we currently have transmission losses of ~67% and could only deliver 0.6 mJ/pulse onto the tissue surface; however, this pulse energy is still

sufficient to ablate these soft tissues with a single manual pass of the beam (beam diameter approximately 200 µm). We have also used the RSA laser to ablate soft tissues such as retina and optic nerve sheath, for which there are established endoscopic laser procedures [15]. These initial results are promising and will be discussed in depth in subsequent publications.

Thus, the RSA laser described here generates pulsed output in the 6- to 7-µm wavelength range that can ablate soft tissues at rates that approach surgical relevance—depending on the chosen procedure and whether endoscopic delivery is necessary. These ablation rates were obtained with typical output pulse energy at multiple times during the laser's first two years of operation. Just as importantly, the incisions produced by this laser are accompanied by very thin regions (< 15 µm) of thermal collateral damage. This combination of robust operation, ablation rates above 10^{-3} mm^3/s and thin regions of collateral damage places the RSA laser in a unique niche with potential applicability in delicate ophthalmic and neurosurgical applications. This potential should only improve with future increases in pulse energy, repetition rate and fiber-optic coupling efficiency—areas in which development is currently in progress. We are also developing automated control of wavelength and operational settings. Collectively, these system enhancements will yield a laser system that is potentially attractive for use in a variety of surgical applications.
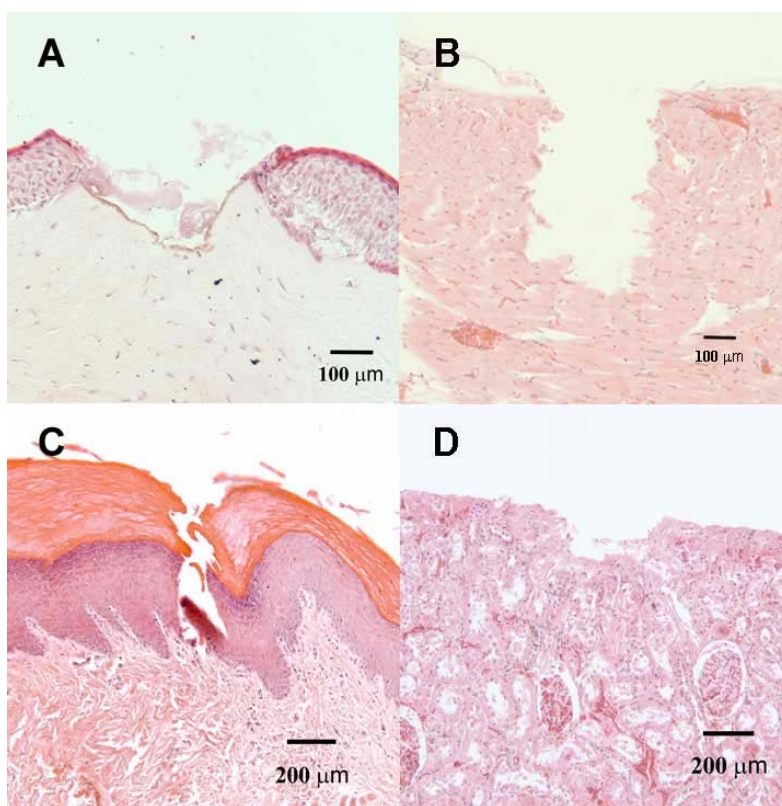

Fig. 3. Histology using H&E stain after RSA laser ablation of excised soft tissues: (**A**) goat cornea, (**B**) rat heart, (**C**) rat skin and (**D**) rat kidney. All ablations were performed at a wavelength of 6.1 µm and a pulse repetition rate of 10 Hz. For (A), the laser was focused onto the cornea surface through air, delivering ~1.9 mJ/pulse to ablate a series of overlapping 10-pulse craters. For (B-D), the laser was delivered through a hollow glass waveguide and handheld probe. This limited delivery to 0.6 mJ/pulse, but allowed the user to manually scan the beam across the tissues as in an actual surgical procedure. Thermal damage is most evident in cornea as the darker region along the crater edge, which is 15-µm thick on average. In the other tissues, thermal damage ranges from minimal to not measureable.